Physical properties of grafted polymer monolayers studied by scanning force microscopy

Koutsos, Vasileios

Chapter 5

Individual Polymer Chains via Mixed Self-Assembled Monolayers: Morphology and Frictional Behavior

In this chapter, we describe a system of mixed self-assembled monolayers of alkanethiols and thiol-terminated polystyrene (PS-SH) chemisorbed on a gold surface from mixed toluene solutions. Topography and friction images were obtained in bad-solvent conditions. We observed single polystyrene coils randomly distributed. The frictional behaviour of the single collapsed chains is investigated and its implications to the image formation are discussed.

5.1 Introduction

Another way for producing polymer monolayers with very low surface coverage is to reduce the number of surface sites available for anchoring. This can be accomplished by simultaneous coadsorption (co-chemisorption) from mixed solutions of short molecules and polymer chains [1]. In case of a polymer which is thiol terminated from both ends, We expect that this method inhibits the formation of loops (or at least it decreases them in number)[1].

Self-Assembling Monolayers (SAM's) of short molecules have proven to be useful for surface modification since they affect interface properties like adhesion and friction [2]. Recently, SAM's derived from organic sulfur compounds have been extensively studied [3]-[13]. Organic thiols chemisorb onto gold surfaces forming a densely packed, crystalline-like structure in which the alkyl chains are slightly tilted with respect to the surface normal. The thiol head group is believed to bind covalently to the gold surface through a gold thiolate bond. The functional tail group is exposed to the free surface. So far, most of the work with these SAM's has been carried out with suitable alkanethiols [14]-

[1]This statement will be verified in chapter 7.

[17], dialkylsulfides and dialkyldisulfides [18, 19]; few studies dealt with thiol-terminated polymers [20]-[23]. The tail group as well as the length of the alkyl chains have been varied in order to obtain the desired properties. The use of mixed SAM's allows even more control over physical and chemical properties of solid surfaces [7, 8].

In this chapter we present the preparation of mixed monolayers of alkanethiols and PS-SH on gold surfaces from two-component solutions and their imaging in bad-solvent conditions using scanning force microscopy (SFM). We acquired both topography and lateral force images. Force modulation measurements were published in the past [24].

We found that when a gold substrate is brought into contact with a solution containing a mixture of short alkanethiols and PS-SH a mixed monolayer is spontaneously formed within which single polymer chains are randomly distributed.

5.2 Experimental Part

5.2.1 Materials

Dodecanethiol (Janssen Chimica) and toluene p.a. (Merck) were used as received. Thiol-terminated polystyrene (PS-SH) was prepared by anionic polymerization [21, 25]. The molecular weight and the molecular weight distribution of the polymer were determined by gel permeation chromatography (GPC) Molecular weight data for the PS_x-SH molecules are given in table 5.1. Flory radii of gyration of the polymer chains in solution (toluene, good solvent for PS) were measured by light scattering using a DAWN DSP-F instrument, at a wavelength of 632.8 nm table 5.1.

Table 5.1: *PS_x-$SH^{(\alpha)}$ Characteristics*

polymer	M_w	M_w/M_n	R_f (nm)
PS_{1400}-SH	144 000	1.20	33.3
PS_{2500}-SH	258 000	1.10	46.9

$^{(\alpha)}$ The subscript refers to the approximate degree of polymerization.

5.2.2 Monolayer Preparation

All the samples were prepared by exposing gold substrates (prepared as described in the subsection 3.2.2) to two-component solutions of PS-SH and dodecanethiol in toluene of the desired composition. A schematic drawing of the mixed-monolayer formation is shown in fig. 5.1. The PS-SH concentration in the solution was kept well below the critical overlap concentration c^* [26]. The adsorption solutions of the desired mole fraction PS-SH (x_{PS-SH}) were prepared by keeping the PS-SH concentration constant and adding the appropriate amount of dodecanethiol. Here x_{PS-SH} equals the ratio of the number of

moles of PS-SH (n_{PS-SH}) and the total number of moles of the two adsorbing components ($n_{PS-SH} + n_{dodecanethiol}$) in the solution:

$$x_{PS-SH} = \frac{n_{PS-SH}}{n_{PS-SH} + n_{dodecanethiol}} \tag{5.1}$$

We used toluene solutions of 1 mg/ml of PS_x-SH. It has been found by employing Ellipsometry, XPS (X-ray Photoelectron Spectroscopy) and SFM in air[2] that the polymer chains begin to adsorb for values of x_{PS-SH} higher than 0.8 [1, 29]. The increase in polymer adsorption at sufficiently high x_{PS-SH} values can be explained by a smaller diffusion coefficient for PS-SH compared to dodecanethiol and the fact that the polystyrene chain in an apolar solvent (toluene) will shield its polar thiol group. Compared to the dodecanethiol molecule, the thiol group in PS-SH therefore has a much lower probability to react with the gold surface. This results in a smaller mole fraction of chemisorbed PS-SH than would be expected from the mole fraction of PS-SH in the adsorption solution under the assumption that both molecules diffuse at the same rate.

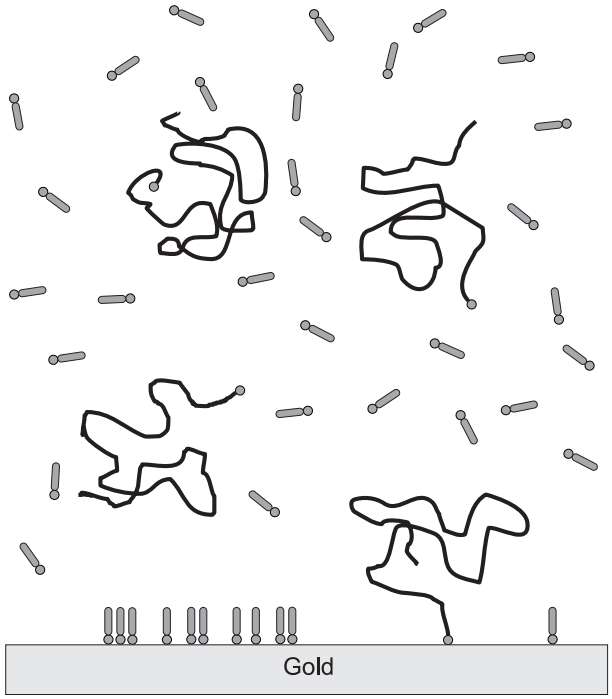

Figure 5.1: *Schematic representation of the mixed monolayer formation from the corresponding two-component solution.*

After 48 hours the substrates were removed from the adsorption solution and immediately rinsed exhaustively with fresh toluene. The samples were dried under a stream of

[2]It is harder to image clearly the polymer chains in ambient conditions beacause of the meniscus forces (exerted by a water condensation between the tip and the sample) that can act as an additional load [27, 28].

argon and were placed in vacuum at 50 ^{o}C for 1 hour, and stored in nitrogen.

XPS measurements and SFM images indicate no adsorption of unmodified polystyrene from a toluene solution onto a gold surface. It has been demonstrated that the adsorption process of modified polystyrene PS-SH (in polymer only solutions) is complete after 24 hours when a polymer concentration of 0.2 to 2 mg/ml is used (molecular weights in the range of 10^3 to 2×10^5 mol/g) [21]. The characteristic chemisorption time for the alkanethiol solutions (for concentrations of about 5 μM) is in the order of some minutes [30].

5.2.3 Scanning Force Microscopy

The scanning force microscopy [31] experiments have been performed under water (bad solvent for PS molecules) using a Topometrix AFM (Explorer). Imaging was performed in the contact mode (tip in contact with the surface) keeping the applied force constant. Within the range of about 1 nN to 5 nN reproducible and similar images were taken. The adhesive force was determined from force-distance curves to be around 2 nN. During attempts to image the monolayer with a negative applied force (applied force $\approx$ adhesive force) the tip usually snapped up out of contact after a few line scans.

In addition to topography images, lateral force images were obtained. While the sample is scanned perpendicular to the long axis of the cantilever, the output of the horizontal two quadrants of the photodiode-detector is measured. In this configuration, the lateral force will cause the cantilever to twist. The degree of twisting can be monitored from the differential signal between the left and right detector and it can be related to the magnitude of the total lateral force.

Commercially available Si_3N_4 (V-shaped, force constant 0.032 N/m) cantilevers were used. The scanning speeds used were in the range of 5 μm/s.

All SFM results displayed excellent reproducibility, and the measurements that are presented here are typical. The images are shown without any processing except levelling.

5.3 Results and Discussion

In fig. 5.2a, c and 5b, d we present the normal force (topography) and the lateral force images, respectively, of mixed monolayers of alkanethiol and PS-SH. Two molecular weights were used: PS_{1400}-SH (fig. 5.2a, b) and PS_{2500}-SH (fig. 5.2c, d). The mole fractions and concentrations in the solution were the same for both polymers ($c = 1$ mg/ml and $x_{PS_{1400}-SH} = x_{PS_{2500}-SH} = 0.85$). The images have been taken simultaneously under water with an applied load of about 1.0 nN. The PS_{1400}-SH polymer is more densely distributed since its molar concentration in the solution was larger in comparison with the molar concentration of PS_{2500}-SH. The polymer islands are clearly imaged, although some of them seem to be deformed and/or partially smeared out. Nevertheless, the majority of the single coils have apparently been subjected to only a slight deformation or none at all and we will concentrate now on their size and shape.

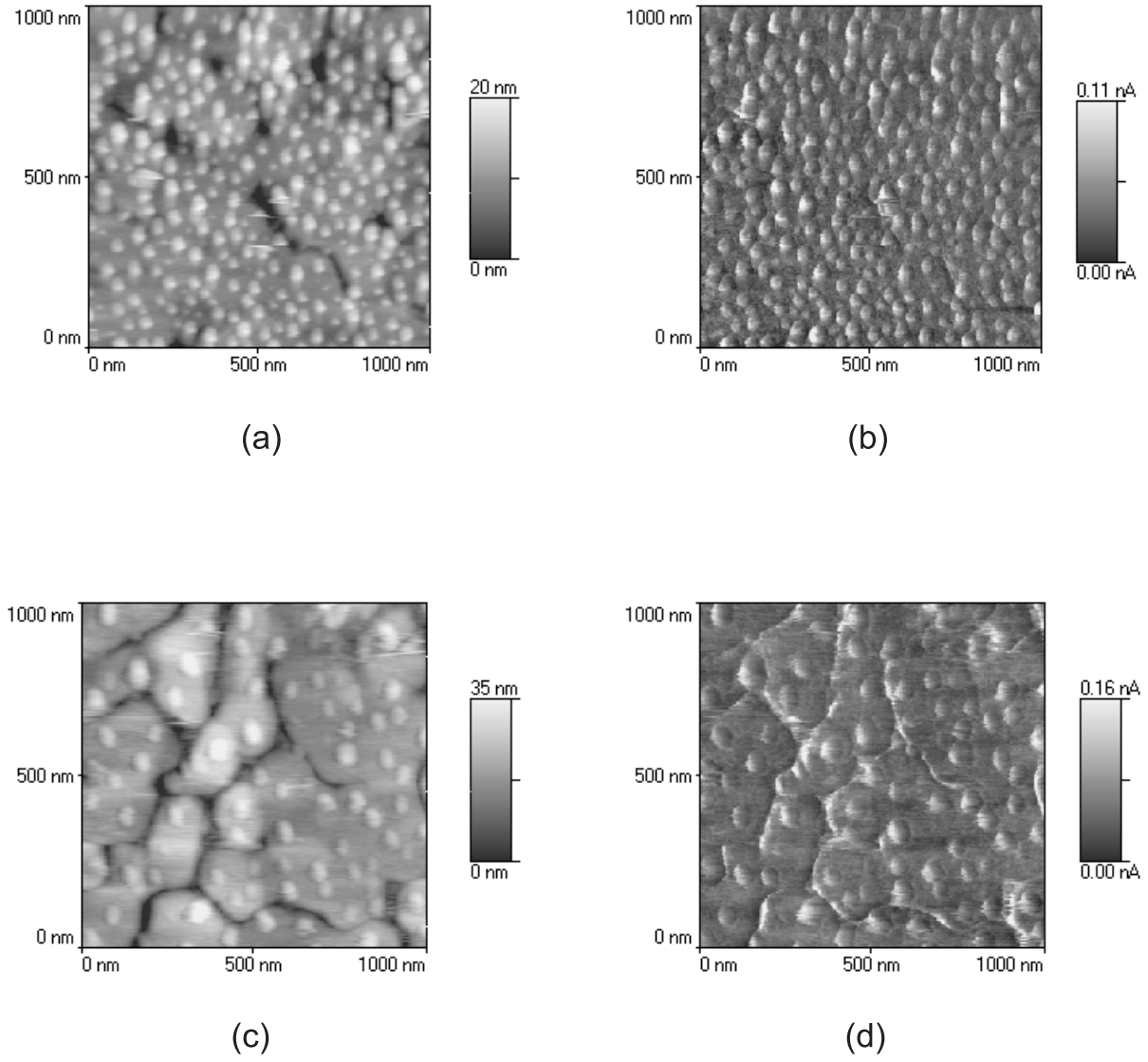

Figure 5.2: *Topographic (a, c) and simultaneously acquired lateral force images (b, d) of a mixed monolayer of alkanethiol and PS-SH. a, b) PS_{1400}-SH, $x_{PS_{1450}-SH} = 0.85$, $c = 1$ mg/ml and c, d) PS_{2500}-SH, $x_{PS_{2600}-SH} = 0.85$, $c = 1$ mg/ml. For the lateral force images: bright/dark appearance indicates high/low lateral force.*

5.3.1 Size and Volume of Single Collapsed Chains

Since we used an applied load of 1 nN we expect that the relatively compliant PS ($E_{PS} = 4$ GPa [38]) will be indented by the stiff tip ($E_{Si_3N_4} = 130 - 150$ GPa [35, 36]) more than the gold substrate[3] ($E_{Au} = 80$ GPa). It is essential to see if there is any considerable difference in the penetration depth for the two materials (SAM+Au and PS globules) since this could affect the measured heights in topography images as it has been described in chapter 2. Based on contact mechanics [33] we evaluated the magnitude of this effect. Applying JKRS theory [34], the penetration depth was found to be about 0.2 nm for the PS globules and 0.1 nm for gold. The heights of the polymer islands are in the range of 5 to 10 nm. Hence, the error in heights due to this effect is about 1 to 2%, which is rather small and was neglected.

We consider (as we did in chapter 3) the shape of a polymer island to be close to a spherical cap (the treatment of small globules in terms of macroscopic quantities is justified even for single collapsed polymer coils; for details see ref. [39]), we can estimate its radius (r) (eq. 3.6) and contact angle (θ) (eq. 3.7) in terms of its apparent width (w_p), height (h) and tip radius (R_t) (see section 2.2).

Knowing the radius and the contact angle of the polymer cap, its volume V_c can be calculated from equation 3.8. We measured the half-width (w_p) and the height (h) of the collapsed chains from corresponding line profiles (fig. 5.3).

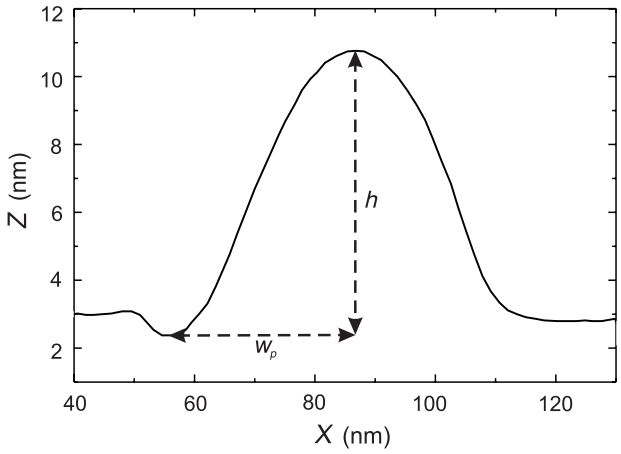

Figure 5.3: *Cross-profile of an undeformed PS_{2500}-SH molecule.*

We considered polymer coils that 1) are well on the flat gold terraces, since polymer images close to edges suffer from artefacts that are not easy to deal with and 2) not heavily deformed. The radii r, the angles θ and the volumes V_c of the polymer islands were calculated from the measured quantities w_p and h via the above equations for each island separately. Taking the density of a collapsed PS chain approximately equal to the usual bulk polystyrene density, we estimated its volume V_t from its molecular weight. In

[3]We assume that SAM's do not change significantly the elastic behavior of solids [37].

table 5.2 we summarize the average measured quantities w_p, h, the average calculated ones r, θ, V_c and the theoretically estimated volumes V_t.

Table 5.2: *Measured and Calculated Average Values for Collapsed Polymer Coils*

polymer	$h^{(a)}$ (nm)	$w_p^{(a)}$ (nm)	$r^{(b)}$ (nm)	$\theta^{(b)}(^o)$	$V_c^{(b)}$ (nm^3)	$V_t^{(c)}$ (nm^3)
PS_{1400}-SH	6.2	26.5	4.7	110 ± 15	320 ± 95	239
PS_{2500}-SH	8.9	31.7	5.9	115 ± 15	678 ± 210	428

$^{(a)}$ measured values from SFM images $^{(b)}$ calculated values based on SFM images $^{(c)}$ estimated values based on the assumption that the polymer density is 1 g/cm^3

We can see that the calculated volumes V_c of the polymer islands are in the range of the theoretically predicted V_t values. However, V_c exceeds V_t by 30%. This can be tentatively attributed to some toluene molecules that were trapped during the collapse of the coil. Some polymer islands occupy volumes close to the volumes that two chains, collapsed together, would occupy. Consequently, we cannot entirely exclude the presence of some polymer islands consisting of two chains.

5.3.2 Conformation and Lateral Deformation of Single Chains

In the profile of fig. 5.3 we can see a small trough *just before* the tip encounters the chain (direction of scanning from left to right). This feature is a general characteristic as can be seen in fig. 5.4 where a zoom in the SFM image of fig. 5.2c is presented.

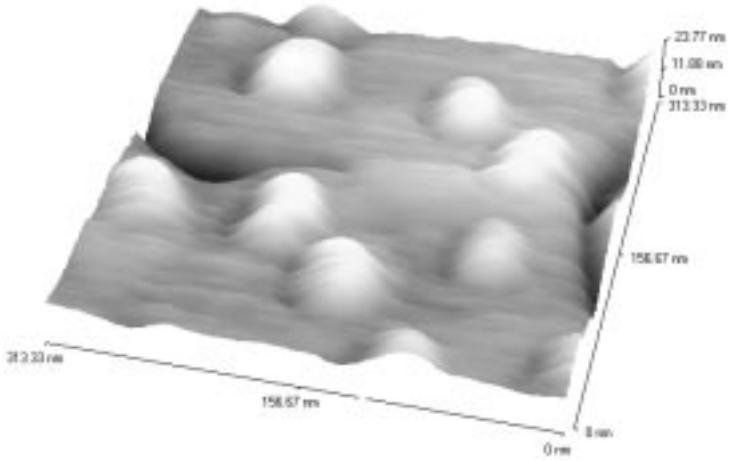

Figure 5.4: *zoom in the image of fig. 4.2c. The direction of scanning from left to right. Troughs can be seen just left of every collapsed chains.*

The appearance of the trough is more prominent and more clearly visible for PS_{2500}-SH than for the lower molecular weight. In fig. 5.5 a typical profile of a deformed collapsed

chain is shown. We see that the size of the trough is larger and that the polymer island is pulled by the tip in the direction of scannings making its shape asymmetric (the slope on the left is less steep than the slope on the right). The average depth of the trough for the PS_{2500}-SH molecules is about 2 nm and its lateral size (in the direction of scanning along the diameter of the chain) varies from about 5 to 15 nm. For the PS_{1400}-SH molecules the trough appears only rarely with depth and lateral size of about 1 nm and 5 nm, respectively. This feature is totally absent when PS-SH is chemisorbed on a bare gold substrate from solutions that do not contain alkanethiols (see chapter 3).

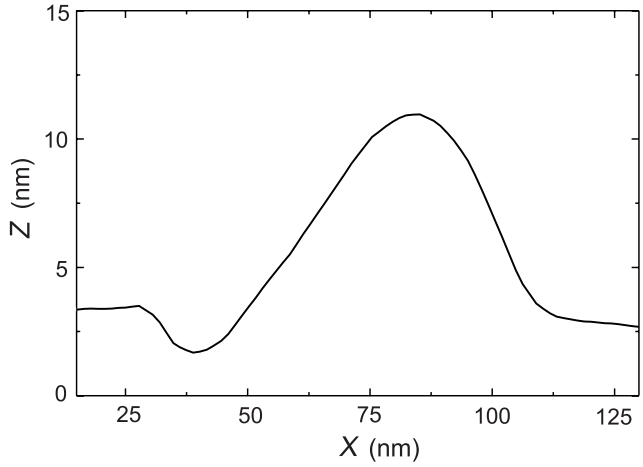

Figure 5.5: *Cross-profile of a deformed and/or dragged PS_{2500}-SH molecule.*

Based on these observations and on the fact that the height of the dodecanethiol SAM is about 2 nm. we associate the appearance of the trough with the area around the grafted chains, unfilled (or partially filled) with dodecanethiols. Because of the unfavourable interactions between the grafted chains and the alkanethiols in the solution we expect a reduced chemisorption of alkanethiols in the vicinity of the grafted coils: in a way, the swollen polymer coil "masks" its neighborhood (fig. 5.6a). When the polymer collapses (fig. 5.6b) its size decreases and because of presence of the alkanethiol layer around it a trough forms. This trough is inaccessible to the tip because the tip radius is much larger. However, it can be imaged, from one side only, when the polymer chain is dragged and/or deformed by the tip in the direction of scanning. In this case, the collapsed chain is pulled over some nanometers by the tip, partially exposing the bare area in the vicinity of the single globule (fig. 5.6c). The dragging and/or deformation of the collapsed polymer chains can be explained partly by the nonideal force control on impact and partly by the larger friction coefficient of PS relatively to that of the alkanethiol SAM. When the tip encounters the polymer, it is transferred from a low-friction region (alkanethiol) to a high-friction one (polymer). Thus, either a) the tip sticks to the polymer and drags it for a short period until the resistance of the polymer via the tether is high enough for the tip to slide and proceed over it, or b) the tip deforms the polymer globule elastically in the

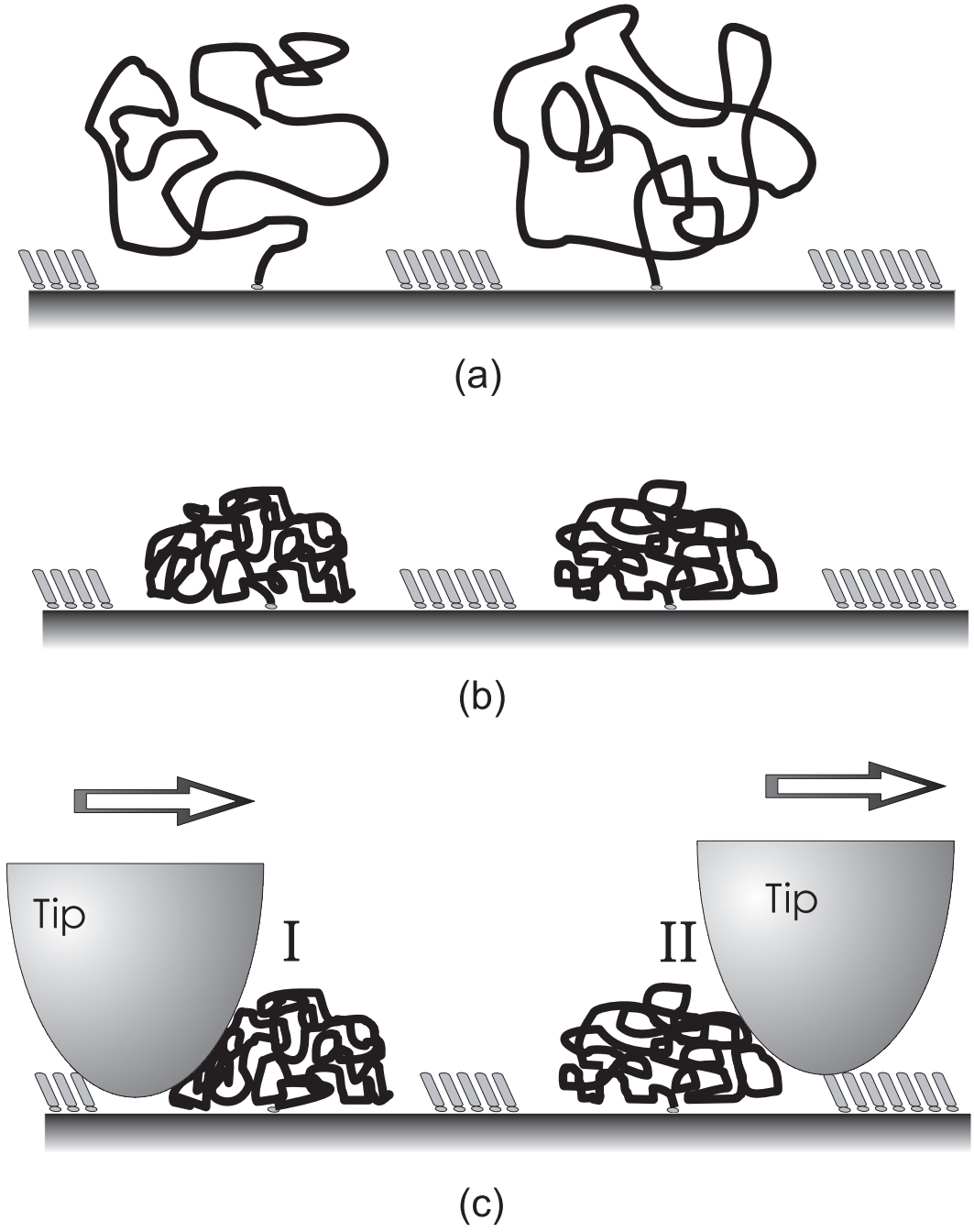

Figure 5.6: *Schematic drawing of a mixed monolayer: a) in solution; In good-solvent conditions the polymer coil is expanded (swollen) and prevents the alkanethiol molecules from adsorbing in its vicinity, b) in bad-solvent conditions, the polymer chains collapse on the surface leaving an empty area around them. c) The imaging process: (I) The polymer globule is dragged and/or deformed by the tip and the widened trough is imaged; (II) due to convolution the trough is not imaged.*

direction of scanning due to relatively high friction on the polymer chain (actually, this effect has been observed in simulations by Aimé et al. [40]), or c) both effects occur. The friction coefficient of CH_3-terminated SAM's has been measured with SFM to be around 0.02-0.05 [41]. The macroscopic friction coefficient of amorphous PS is 0.515 [38] but it would be more relevant to measure the local friction coefficient on the polymer globules. This can be accomplished by addressing lateral force profiles and topography profiles obtained simultaneously.

5.3.3 Friction Measurements

In fig. 5.7 we present a lateral force profile (a) and the corresponding, simultaneously taken topographical one (b) of a single collapsed chain. The frictional force resembles the first derivative of topography ($\frac{dz}{dx}$) i.e. a maximum (minimum) appears in friction when the slope of topography is positive (negative). A qualitative explanation of this result is presented in fig. 5.8. We depict the twisting of the cantilever while scanning a spherical globule. Its size is overexagerated for the sake of the argument. When the tip is ascending the polymer globule, it is twisted opposite to scanning direction because of the positive slope of the topography; hence, a lateral force is exerted on the tip, opposite to scanning direction. During the tip's descent from the globule, the cantilever is twisted in the direction of scanning; hence, a lateral force is exerted on the tip in the scanning direction.

Haugstad et al. [42] showed that in case of constant (vertical) cantilever deflection the total torque τ that is exerted on the cantilever is given by [43]:

$$\tau \approx F_l L(\frac{dz}{dx} + \mu_0) \tag{5.2}$$

where F_l is the applied normal load, which remains constant, L is the distance between the principal cantilever axis and the vertex of the spherical tip and μ_0 is the coefficient of friction. $\frac{dz}{dx}$ is evaluated at the point of contact. This model explains why the frictional signal varies as the first derivative of topography.

We will try now, to recover the basic characteristics of the friction signal (profile in fig. 5.7a) using equation 5.2. Curve α in fig. 5.9 depicts the numerically calculated first derivative of the topographical profile of fig. 5.7b. The curve is quite symmetric in contrast to the measured friction profile where the maximum is much more pronounced than the minimum. However, one should take into account the higher friction coeficient of the polymer globule (curve β) (as one would expect intuitively and equation 5.2 also predicts). The combined result is curve γ. We observe that the maximum is indeed more pronounced. Nevertheless, the same kind of measured friction profiles has been observed even in cases of low friction protruding surfaces (for example [42]). Thus, there should be a more general explanation: Due to the finite response time of the feedback, the tip "collides" onto the protrusion and a higher cantilever torsion is produced. Thus, we expect that equation 5.2 would not hold in the region of the tip-globule first contact. However,

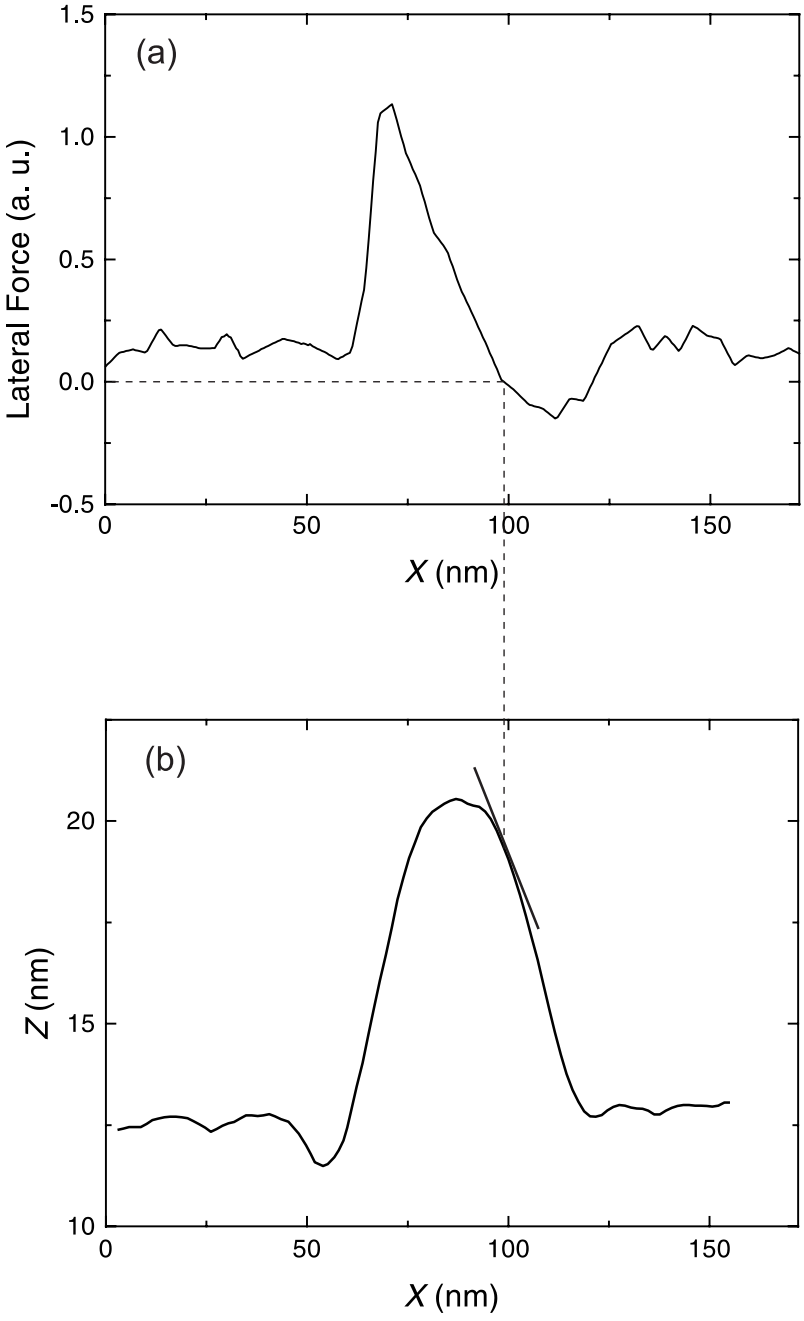

Figure 5.7: *Simultaneously obtained cross-profiles along a single polymer chain: lateral force (a) and topography (b) At the first point of zero total lateral force (zero torsion) the corresponding negative slope of the topography is equal to the coefficient of friction* μ_0.

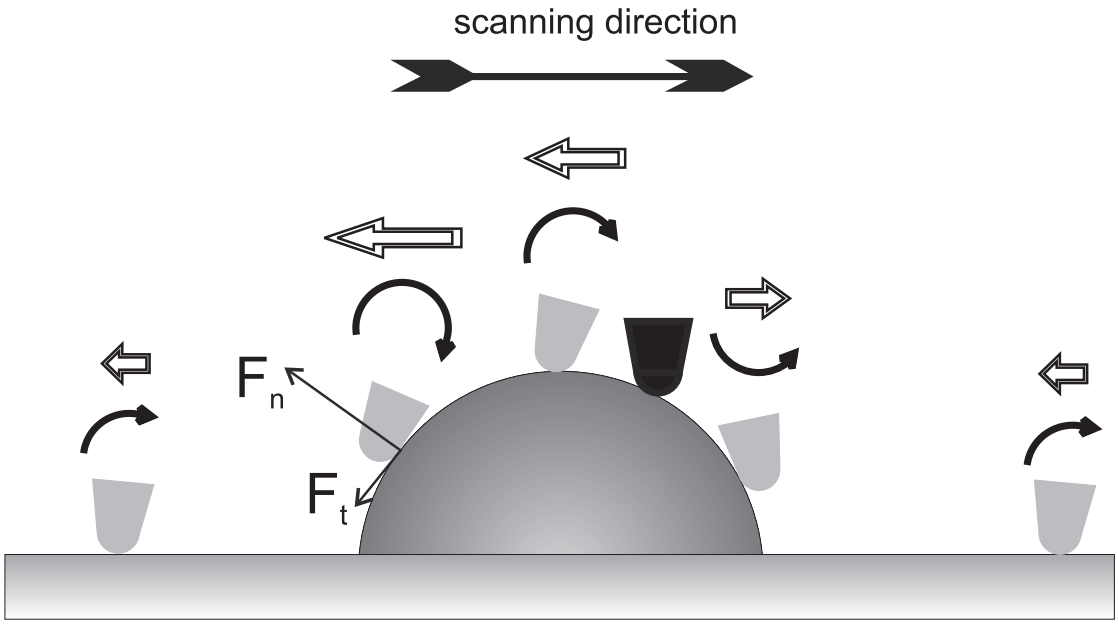

Figure 5.8: *Schematic drawing of the cantilever twisting during left-to-right scanning. The sign and magnitude of the associated torque about the principal axis are indicated above each respective loaction. The vectors represent the corresponding lateral force. It is assumed that the friction force is higher on the polymer globule. Notice that during the descent of the tip from the globule there is a point where the total torque (lateral force) vanishes (black tip). In a way, the topography slope counterbalance the local friction.*

it is expected to hold during the tip's descent from the globule.

It follows from equation 5.2 that at the point where τ vanishes (i.e. lateral force vanishes) the coefficient of friction is equal to the negative slope of the topography. This is actually happening once during the descent of the tip from the polymer coil, at the point where the slope is -0.26; hence $\mu_0 = 0.26$. Using this method, we measured the local friction coefficient for several single collapsed chains: we found an average value of about 0.3. which is in the range of the macroscopic value, although 40% smaller. We will investigate the origin of this difference in the next chapter. We note that this is the *local* friction coefficient without including the effect of the roughness; that is, the ratio of the force F_n exerted on the spherical tip normal to its microscopic surface and the tangential force F_t (fig. 5.8). The friction coefficient that is measured by usual tribological experiments 1) is an average of a lot of asperities 2) the load (friction force) is normal (tangential) to the macroscopic surface.

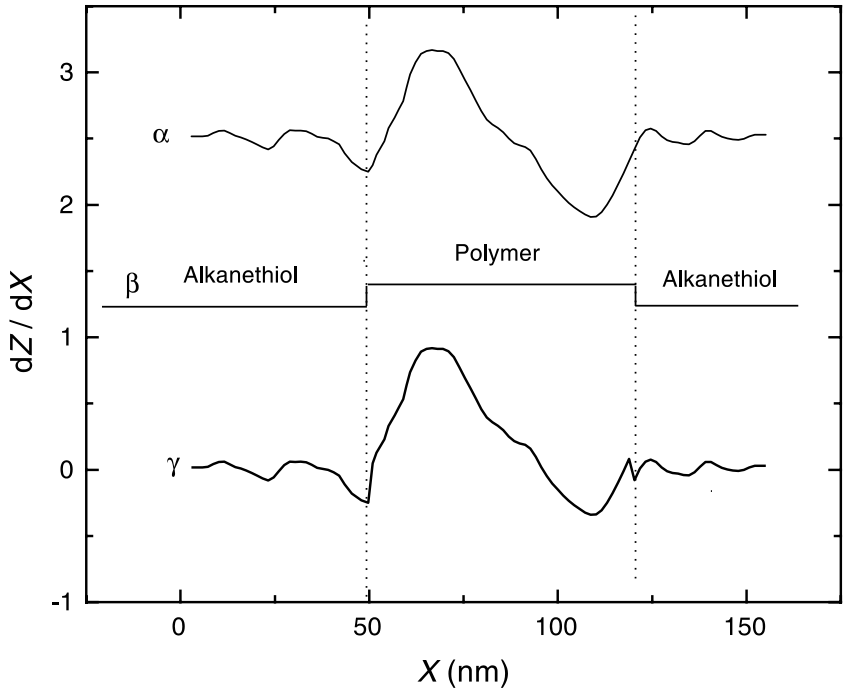

Figure 5.9: *Curve α: first derivative of the topography profile in fig. 5.7b (+ arbitrary offset); curve β: friction signal of an ideally flat -alkanethiol+polymer- surface (+ arbitrary offset); curve γ: superpostion of α and β.*

To our knowledge this is the first report of the local friction coefficient on a single polymer chain. This relatively high friction coefficient, compared with the friction coefficient of the alkanethiol SAM, can account for the deformation and/or dragging of the single polymer globules in the direction of scanning.

5.4 Conclusions

The spontaneous adsorption of PS-SH molecules and alkanethiols onto Au surfaces from mixed solutions in toluene resulted in an adsorbate containing isolated polymer chains randomly distributed in a SAM of alkanethiols. The majority of the collapsed chains exhibited structural stability, although some of them were deformed and/or dragged by the tip during imaging. This effect can be attributed partly to the abrupt surface elevation and partly to the high local friction coefficient of single PS globules, which was measured to be in the range of that of bulk polystyrene.

References

[1] *Direct View of Thin Polymer Films with Scanning Force Microscopy* Grim, K. Ph.D. Thesis in Rijksuniversiteit Groningen.

[2] Ulman, A. *An introduction to Ultrathin Organic Films*, Academic Press: San Diego, CA, **1991**.

[3] Porter, M. D.; Bright, T. B.; Allara, D. L.; Chidsey, C. E. D. *J. Am. Chem. Soc.* **1987**, *109*, 3559.

[4] Bain, C. D.; Troughton, E. B.; Tao, Y.-T.; Evall, J.; Whitesides, G. M.; Nuzzo, R. G. *J. Am. Chem. Soc.* **1989**, *11*, 321.

[5] Nuzzo, R. G.; Dubois, L. H.; Allara, D. L. *J. Am. Chem. Soc.* **1990**, *112*, 558.

[6] Dubois, L. H.; Zegarski, B. R.; Nuzzo, R. G. *J. Am. Chem. Soc.* **1990**, *112*, 570.

[7] Laibinis, P. E.; Fox, M. A.; Folkers, J. P.; Whitesides, G. M. *Langmuir* **1991**, *7*, 3167.

[8] Bertilsson, L.; Liedberg, B. *Langmuir* **1993**, 9, 141.

[9] Grunze, M. *Physica Scripta* **1993**, *T49*, 711.

[10] Kim, Y.-T.; McCarley, R. L.; Bard, A. J. *J. Phys. Chem.* **1992**, *96*, 7416.

[11] McCarley, R. L.; Kim, Y.-T.; Bard, A. J. *J. Phys. Chem.* **1993**, *97*, 211.

[12] Widrig, C. A.; Alves, C. A.; Porter, M. D. *J. Am. Chem. Soc.* **1991**, *113*, 2805.

[13] Alves, C. A.; Smith, E. L.; Porter, M. D. *J. Am. Chem. Soc.* **1992**, *114*, 1222.

[14] Zak, J.; Yuan, H.; Ho, M.; Woo, L. K.; Porter, M. D. *Langmuir* **1993**, *9*, 2772.

[15] Caldwell, W. B.; Chen, K.; Mirkin, C. A.; Babinec, S. J. *Langmuir* **1993**, *9*, 1945.

[16] Sabatani, E; Cohen-Boulakia, J.; Bruening, M.; Rubinstein, I. *Langmuir* **1993**, *9*, 2974.

[17] Häussling, L.; Ringsdorf, H.; Schmitt, F.-J.; Knoll, W. *Langmuir* **1991**, *7*, 1837.

[18] Spinke, J.; Liley, M.; Schmitt, F,-J.; Guder, H. -J.; Angermaier, L.; Knoll, W. *J. Chem. Phys.* **1993**, *99*, 7012.

[19] Lang, H.; Duschl, C.; Vogel, H. *Langmuir* **1994**, *10*, 197.

[20] Niwa, H.; Shimoguphi, M.; Higashi, N. *J. Coll. Interf. Sci.* **1992**, *148*, 592.

[21] Stouffer, J. M.; McCarthy, T. J. *Macromolecules* **1988**, *21*, 1204.

[22] Sun, F.; Castner, D. G.; Grainger, D. W. *Langmuir* **1993**, *9*, 3200.

[23] Whitesell, J. K.; Chang, H. K. *Science* **1993**, *261*, 73.

[24] Akari, S.; v.d. Vegte, E. W.; Grim, P. C. M.; Belder, G. F.; Koutsos, V.; ten Brinke, G.; Hadziioannou, G. *Appl. Phys. Lett.* **1994**, *65*, 1915.

[25] Tang, W. T. *Study of block copolymer micelles in dilute solution by light scattering and fluorescence spectroscopy*, dissertation Stanford University: **1987**, p.28-33.

[26] de Gennes, P.-G. *Scaling Concepts in Polymer Physics*, Cornell University Press: Ithaca, NY, 1979.

[27] Weisenhorn, A. L.; Hansma, P. K.; Albrecht, T. R.; Quate, C. F. *Appl. Phys. Lett.* **1989**, *54*, 2651.

[28] Burnham, N. A.; Colton, R. J.; Pollok H. M. *J. Vac. Sci. Technol.* **1991**, *A9*, 2548.

[29] Koutsos, V.; van der Vegte, E. W.; Grim, P. C. M.; Hadziioannou, G. submitted to *macromolecules*.

[30] a) Shimazu, K.; Yag, I.; Sato, Y; Uosaki, K. *Langmuir* **1992**, *8*, 1385. b) Karpovich, D. S.; Blanchard, G. J. *Langmuir* **1994**, *10*, 3315. c) Grunze, M. *Physica Scripta* **1993**, *T49*, 711.

[31] Binnig, G.; Quate, C. F.; Gerber, Ch. *Phys. Rev. Lett.* **1986**, *56*, 930.

[32] Zheng, X.-Y.; Youzhen D.; Bottomley, L. A. *J. Vac. Sci. Technol.* **1995**, *B13(3)*, 1320.

[33] (a) Johnson K. L. *Contact Mechanics*, Cambridge University Press, 1985. (b) Horn, R. G.; Israelachvili J. N.; Pribac F. *J. Coll. Interf. Sci.* **1987**, *115(2)*, 480.

[34] (a) Johnson, K. L.; Kendal K.; Roberts A. D. *Proc. R. Soc. Lond. A* **1971**, *324*, 301. (b) Sperling, G. Ph.D. Thesis in Karlsrule Technical High School, 1964.

[35] Petersen, K. E. *Proc. IEEE* **1982**, *70*, 420.

[36] Sader, J. E.; Larson, I.; Mulvaney, P.; White, L. R. *Rev. Sci. Instrum.* **1995**, *66*, 3789.

[37] Thomas, R. S.; Houston, J. E.; Michalske T. A.; Crooks, R. M. *Science* **1993**, *259*, 1883.

[38] *Polymer Handbook*, third edition, edited by J. Brandrup and E. H. Immergut, Wiley: New York, 1989.

[39] Johner, A.; Joanny J. F. *J. Phys. II* **1991**, *1*, 181.

[40] Aimé J. P.; Elkaakour, Z; Gauthier S.; Michel D.; Bouhacina T.; Curély J. *Surface Science* **1995**, *329*, 149.

[41] Tsukruk, V. V.; Everson, M. P.; Lander, L. M.; Brittain, W. J. *Langmuir* **1996**, *12*, 3905.

[42] Haugstad, G.; Gladfelter, W. L. *Langmuir* **1993**, *9*, 3717.

[43] This model applies only if the factor $\frac{R_t}{L}(1 + (\frac{dz}{dx})^2)^{1/2}$ is sufficiently small (≤ 0.1). This holds since $R_t/L \approx 0.02$ and $\frac{dz}{dx} \leq 5$.